S values for a monkey computational model for internally distributed radiation sources

Daniel D. Lee[1], Jae Won Jung[2]

[1]Thomas S. Wootton High School, Rockville, MD, 20850, USA

[2]Department of Radiation Oncology, East Carolina University, Greenville, NC, 27858, USA

Submitted to Radiation Physics and Chemistry

Abstract

Background: In the field of nuclear medicine, monkeys have been instrumental in advancing our understanding of how radioactive materials behave within a living organism. However, comprehensive dosimetric data, including S values, for various source and target regions and radionuclides remain limited. The current study is aimed to develop a comprehensive library of S values, a critical dose metric, by utilizing a computational monkey model in conjunction with Monte Carlo radiation transport methods.

Methods: We developed an S-value library for the anatomical monkey model through the following process. First, we computed specific absorbed fractions (SAFs) for 35 sources and 35 target organs using the general-purpose Monte Carlo radiation transport code, MCNP6. Monte Carlo simulations were performed for both photons and electrons, covering 27 monoenergetic bins ranging from 0.01 to 10 MeV. Next, we derived the S-values from the SAFs for photons and electrons by incorporating energy spectrum data for 299 radionuclides, as provided by ICRP Publication 107.

Results: We created a library of S values for 35 source and 35 target organs derived from the SAFs combined with the energy spectrum of 299 commonly used radionuclides provided by ICRP Publication 107. The differences in self-absorption S values for the large organs likely stem from the type of particles: positron/beta vs. gamma. Crossfire S values mirror the trends seen in SAFs, particularly in relation to the inter-organ distances between source and target regions. Determining whether the monkey model accurately represents human models for specific age groups remains challenging.

Conclusion: We developed an extensive S value library for 299 commonly used radionuclides based on a monkey anatomical model, utilizing Monte Carlo radiation transport methods. This S value library is expected to be a valuable resource for estimating organ doses in monkeys when paired with radionuclide distribution data across their anatomy.

Introduction

Monkeys have been extensively used in a wide range of research fields due to their significant genetic and physiological similarities to humans (Phillips et al., 2014; Weerts et al., 2007). This makes them ideal models for studying complex biological processes. Particularly in the field of nuclear medicine, monkeys have been instrumental in advancing our understanding of how radioactive materials behave within a living organism (Bartlett et al., 2010; Brown et al., 2007; Marti-Climent et al., 2015). Researchers have used monkeys to study the distribution, absorption, and interaction of radiation with various organs, gaining valuable insights into the biological impact of radiation exposure. These findings are critical for establishing dose-response relationships and informing safety protocols, ultimately improving the safety and effectiveness of radiation-based diagnostic and therapeutic procedures in human medicine. The use of monkeys in this research has provided a better understanding of radiation behavior within the body, offering insights that are directly translatable to human health.

Both experimental research and computer simulations involving monkeys have greatly advanced our understanding of biological processes and radiation effects. Monkeys are commonly used in radiation biology studies where human experimentation is impractical or unethical. These studies are crucial for assessing safety, efficacy, and potential side effects before progressing to human trials. Experimental research provides direct biological data, while computer simulations, based on monkey data (Takamura et al., 2023; Xie et al., 2020), offer precise energy deposition estimates for internal organs and tissues when radionuclides are distributed within the monkey's anatomy. This combined approach improves the accuracy of dose assessments in radiation research, helping to bridge the gap between experimental results and their application to human health in nuclear medicine. However, comprehensive dosimetric data, including S values for various source and target regions and radionuclides, remain limited.

The current study aimed to develop a comprehensive library of S values, a critical dose metric, by utilizing a computational monkey model in conjunction with Monte Carlo radiation transport methods. We first calculated a database of specific absorbed fraction (SAF) and derived S values from them using the energy spectrum data of frequently used radionuclides. We also compared our results with those derived from the reference computational human phantoms.

Material and method

We developed an S-value library for the monkey anatomical model through the following process. First, we computed specific absorbed fractions (SAFs) for 35 sources and 35 target organs using the general-purpose Monte Carlo radiation transport code, MCNP6. Monte Carlo simulations were performed for both photons and electrons, covering 27 monoenergetic bins ranging from 0.01 to 10 MeV. Next, we derived the S-values from the SAFs for photons and electrons by incorporating energy spectrum data for 299 radionuclides, as provided by ICRP Publication 107 (ICRP, 2008).

Computational monkey model

We utilized a computational monkey model developed by Chung et al. (Chung et al., 2019), based on a female rhesus monkey measuring 76 cm in height and weighing 4.3 kg. Polygon-mesh organ models were obtained from the Electronics and Telecommunications Research Institute website[1] and imported into the 3D modeling software Rhinoceros (Robert McNeel & Associates, Seattle, WA) to create a whole-body surface-format phantom, consisting of 180 organs and tissues. To enable compatibility with a Monte Carlo transport code, we converted the surface-format phantom into a voxel model using an in-house voxelization code, assigning each structure a specific voxel tag. The final model included 180 segmented anatomical structures. Figure 1 presents frontal and rear oblique views of the monkey model with labeled organs, where the skin, muscle, fat, and skeleton were removed in the oblique view to better visualize the internal organs. The voxel model had an array size of 233 x 152 x 761 voxels in the X, Y, and Z directions, with a total file size of approximately 27 MB.

Monte Carlo radiation transport

We conducted radiation transport simulations using the general-purpose Monte Carlo code MCNP6 (Goorley et al., 2016). The voxel phantom generated in the previous step was converted into a lattice format in ASCII, compatible with MCNP6. Since elemental composition and density data for monkey organs and tissues are not readily available, we used human data from ICRP (ICRP, 2020) as a surrogate. Mono-energetic photons and electrons were emitted within the source organ, and the radiation energy deposited in the target organ was calculated using the *F8 energy deposition tally card, which tracks and scores secondary electrons. Energy bins from 0.01 to 10 MeV were employed for source energy sampling. The simulation was performed on a Mac Studio with a 24-core CPU and 128 GB of RAM, with photon and electron SAF calculations taking approximately three months to complete.

---

[1] https://www.data.go.kr/en/data/15074162/fileData.do

Calculation of specific absorbed fraction

The calculation of organ doses from internally-deposited radionuclides follows the Medical Internal Radiation Dose (MIRD) schema (Bolch et al., 2009). In total, 35 source organs and 35 target organs were defined for Monte Carlo calculations (Table 1). We then computed absorbed fraction (AF), representing the portion of particle energy emitted from a source region r_S that is deposited in a target region r_T, across 1,225 source-target combinations using the following equation:

$$\phi(r_T \leftarrow r_S) \tag{1}$$

The absorbed fraction (AF) must be calculated for each type of particle (e.g., photon, electron) when a radionuclide emits multiple particles within its energy spectrum. We calculated self-absorption AFs for cases where the source and target organs were the same and crossfire AFs for cases where the source and target organs were different.

Next, the specific absorbed fraction (SAF) in units of kg^{-1} is then obtained by dividing the AF by the mass of the target region m_{r_T}, as demonstrated in the following equation:

$$\Phi(r_T \leftarrow r_S) = \frac{\phi(r_T \leftarrow r_S)}{m_{r_T}} \tag{2}$$

We compared self-absorption SAFs between two groups of organs: those with small masses (less than 10 g) and those with large masses (over 100 g). Additionally, we analyzed crossfire SAFs by comparing scenarios where the source organ was nearby (e.g., source in the stomach) versus distant (e.g., source in the thyroid) from the target organs, specifically focusing on major gestational organs.

Calculation of S values for selected radionuclides

Finally, we derived a library of S values (mGy/MBq-s), absorbed dose to a target region per unit cumulated activity in a source region, using the SAFs combined with the energy spectrum of major radionuclides using the following equation:

$$S(r_T \leftarrow r_S) = \sum_{i=1}^{n} y_i E_i \cdot \Phi(r_T \leftarrow r_S) \tag{3}$$

where y_i is the probability of emission of radiation type i with the energy E_i of a given radionuclide, and $\Phi(r_T \leftarrow r_S)$ is the SAF for a source region r_S and a target region r_T. We selected 299 of the most commonly used radionuclides in diagnostic nuclear medicine (Villoing et al., 2020) from over 1,000 radionuclides listed in ICRP Publication 107 (ICRP, 2008). Photon and electron yield and energies were separately extracted from the report. SAF values for photons and electrons were then interpolated to match the extracted photon and electron energies, respectively, in order to calculate the corresponding S values.

We compared S values calculated for Tc-99m distributed in the stomach and urinary bladder with those for the 1-year, 10-year, and adult ICRP reference phantoms, which were extracted from the National Cancer Institute dosimetry system for Nuclear Medicine (NCINM) dose calculator (Villoing et al., 2022).

Results

Specific absorbed fraction

A comprehensive library of photon and electron SAFs, consisting of over 66,000 values for 35 source and 35 target organs across 27 energy bins (ranging from 0.01 to 10 MeV), has been compiled and utilized to calculate S values, which will be detailed in the following section. The complete SAF dataset is available in Excel format in the Supplementary Material, and key SAFs for photon sources are highlighted below.

Figure 2A shows the self-absorption photon SAFs for small organs (tongue, spleen, gall bladder, and trachea) with the mass less than 10 g (Table 1). The gall bladder exhibited the highest value at 0.01 MeV with a value of 624 kg^{-1} followed by the spleen at 362 kg^{-1} and the trachea at 199 kg^{-1}. The tongue recorded the lowest value at 0.01 MeV with a value of 109 kg^{-1}. At 10 MeV, the spleen showed the highest value at 0.485 kg^{-1} while the gall bladder and tongue had similar values of 0.4072 kg^{-1} and 0.3939 kg^{-1}, respectively. The trachea displayed the lowest value at 10 MeV, with a value of 0.2901 kg^{-1}.

The self-absorption photon SAFs for large organs (stomach, liver, small intestine, and large intestine) with the mass greater than 100 g are presented in Figure 2B. At 0.01 MeV, the liver exhibited the highest self-absorption, with values of 6.9917 kg^{-1} and 0.103 kg^{-1} at both 0.01 and 10 MeV, respectively, indicating that it absorbs a significant portion of radiation internally. The small intestine also showed a moderate self-absorption value, with SAFs of 2.7775 kg^{-1} at 0.01 MeV and 0.0799 kg^{-1}at 10 MeV. The stomach and large intestine displayed similar self-absorption levels at 2.0702 kg^{-1} and 2.0531 kg^{-1} at 0.01 MeV, respectively. At 10 MeV, the stomach and large intestine show quite different SAFs of 0.0675 kg^{-1} and 0.055 kg^{-1}, respectively.

The crossfire photon SAFs for the gastrointestinal organs (liver, small intestine, large intestine, and spleen) are shown in Figure 3A when the photon source is in the stomach, which is proximate to the target organs. All organs show the maximum SAFs around 0.03 MeV. Among the organs analyzed, the spleen showed the highest SAF with a value of 0.3134 kg^{-1}. The liver followed with an SAF of 0.2779 kg^{-1}. The small intestine had an SAF of 0.1624 kg^{-1} and the large intestine exhibited the lowest SAF at 0.0198 kg^{-1}.

When photon source is distributed in the thyroid, far from the target organs (liver, small intestine, large intestine, and spleen) (Figure 3B), the maximum SAFs were observed around 0.06 MeV. The

liver exhibited the highest SAF at 0.0134 kg^{-1} followed by the spleen with an SAF of 0.0038 kg^{-1}. The small intestine had an SAF of 0.0020 kg^{-1} and the large intestine had the lowest SAF at 0.0006 kg^{-1}.

S values for monkey model

We created a library of S values for 35 source and 35 target organs derived from the SAFs combined with the energy spectrum of 299 commonly used radionuclides provided by ICRP Publication 107. The full dataset is provided in the Supplementary Material as an Excel file. S values for major source and target combinations (stomach, small intestine, liver, large intestine, esophagus, urinary bladder, lung, heart, kidney, and brain) are tabulated for the source radionuclides of Ga-68, I-123, I-131, In-111, Lu-177, and Tc-99m in Table 2-7, respectively. The major radiation type and average energy is positron 890 keV (Ga-68), gamma 159 keV (I-123), beta 192 keV (I-131), gamma 208 keV (In-111), beta 133 keV gamma 160 keV (Lu-177), and gamma 140 keV (Tc-99m).

The self-absorption S values for different radionuclides when the stomach is the source region show considerable variation. For example, Ga-68 has the highest S value (2.7e-4 mGy/MBq-s), while Tc-99m has the lowest (9.19e-6 mGy/MBq-s).

When considering the crossfire S values (mGy/MBq-s) for different organs with Tc-99m distributed in the stomach (Table 6), the highest S value is found in the stomach itself (9.19E-06), which is anticipated since it serves as the primary site of radiopharmaceutical localization. The liver and small intestine exhibit significant S values of 1.92E-06 and 1.34E-06, respectively, likely due to their proximity to the stomach. Organs such as the kidney and heart also show moderate S values (1.19E-06 and 1.10E-06, respectively). The brain and urinary bladder exhibit the lowest S values (9.28E-08 and 4.61E-08), indicating minimal radiation dose, as these organs are anatomically distant from the source organ.

S value comparison with ICRP reference phantoms

Figures 4 presents the comparison of S values for the stomach, small intestine, liver, large intestine, esophagus, lung, heart, kidney, and brain between the monkey model and the ICRP reference phantoms (1-, 10-year-old, and adult) for Tc-99m when the source is in the stomach (Figure 4A) and urinary bladder (Figure 4B).

The comparison of S values when Tc-99m is distributed in the stomach between a monkey model and ICRP reference human phantoms (Figure 4A) highlights significant differences across age groups. The S values for the 1-year-old human phantom shows only 3% (median) greater than those of the monkey model. In contrast, the 10-year-old and adult human models show 59% (median) and 71% (median) greater S values compared to the monkey model, respectively.

When comparing S values for Tc-99m in the urinary bladder between the monkey model and ICRP reference phantoms (Figure 4B), there are again substantial differences across age groups. The S values from the monkey model are 272% (median) greater than those of the 1-year-old human

phantom. In contrast, the 10-year-old and adult phantoms show 35% (median) and 41% (median) smaller S values compared to those of the monkey model.

Discussion

The strength of this paper lies in its pioneering effort to provide the first detailed S-value calculations specifically tailored to a monkey anatomical model. This represents a significant step forward in the field, as previous studies primarily focused on human models. Additionally, the paper offers a comprehensive list of source-target organ combinations, covering a total of 35 different organs, which enhances the accuracy and depth of its findings. By basing the radionuclide selections on the ICRP Publication 107 (ICRP, 2008), the study also ensures that its methods are aligned with widely accepted standards, further reinforcing the credibility and relevance of its results.

We observed from SAFs that self-absorption is influenced by both organ size and mass. At low energies, SAFs for both small and large organs are primarily determined by the mass of the target organ, as SAFs are calculated by dividing AFs by the target organ mass. However, at higher energies, while large organs continue to follow this mass-dependent trend, SAFs for smaller organs become more reliant on AFs, which are significantly impacted by the amount of radiation escaping the organ. For crossfire SAFs, the inter-organ distance between the source and target organs plays a key role, with SAFs decreasing as the distance—and consequently, radiation attenuation—increases.

The differences in self-absorption S values for the large organs (Table 2-7) likely stem from the type of particles: positron/beta vs. gamma. Positron and beta sources typically result in greater self-absorption S values, as seen with Ga-68, I-131, and Lu-177. On the other hand, radionuclides emitting gamma radiation, such as Tc-99m, correspond to lower self-absorption S values. These variations are important for optimizing radionuclide selection based on the desired radiation dose distribution in nuclear medicine procedures. Crossfire S values mirror the trends seen in SAFs, particularly in relation to the inter-organ distances between source and target regions.

The comparison of S values between the monkey models and ICRP reference human models suggests that the monkey model more accurately reflects the self-absorption S values of the 1-year-old phantom but resembles the crossfire S values of the 10-year-old phantom. Consequently, it is challenging to definitively determine whether the monkey model adequately represents human models for specific age groups.

We acknowledge several limitations in the current work. First, for the sake of simplifying our calculations, we combined the brain substructures into a whole brain, even though the original segmentation provides a more detailed breakdown of the individual substructures. We are actively working on addressing this by conducting Monte Carlo simulations that focus specifically on these

distinct brain substructures. Second, the S-values calculated in this study are tailored to the specific monkey anatomical model we employed, meaning there could be variations when applying these results to other monkey models. Such differences might arise due to variations in target organ mass and inter-organ distances across different anatomical models, which should be considered in future studies. Lastly, we did not derive absorbed dose coefficients, from which organ dose can be estimated by multiplying administered activity, because monkey-specific biokinetic models are not available to date. Human biokinetic data may be used for the purpose.

Conclusions

We developed an extensive S value library for 299 commonly used radionuclides based on a monkey anatomical model, utilizing Monte Carlo radiation transport methods. Our analysis revealed that self-absorption S values depend on the type and energy of the radiation, while crossfire S values are influenced by the inter-organ distances between source and target organs. Determining whether the monkey model accurately represents human models for specific age groups remains challenging. Nonetheless, this S value library is expected to be a valuable resource for estimating organ doses in monkeys when paired with radionuclide distribution data across their anatomy.

References

Bartlett, R.M., Nickles, R.J., Barnhart, T.E., Christian, B.T., Holden, J.E., DeJesus, O.T., 2010. Fetal Dose Estimates for 18F-Fluoro-l-Thymidine Using a Pregnant Monkey Model. Journal of Nuclear Medicine 51, 288–292. https://doi.org/10.2967/jnumed.109.068734

Bolch, W.E., Eckerman, K.F., Sgouros, G., Thomas, S.R., 2009. MIRD Pamphlet No. 21: A Generalized Schema for Radiopharmaceutical Dosimetry—Standardization of Nomenclature. J Nucl Med 50, 477–484. https://doi.org/10.2967/jnumed.108.056036

Brown, A.K., Fujita, M., Fujimura, Y., Liow, J.-S., Stabin, M., Ryu, Y.H., Imaizumi, M., Hong, J., Pike, V.W., Innis, R.B., 2007. Radiation Dosimetry and Biodistribution in Monkey and Man of 11C-PBR28: A PET Radioligand to Image Inflammation. Journal of Nuclear Medicine 48, 2072–2079. https://doi.org/10.2967/jnumed.107.044842

Chung, B.S., Jeon, C.-Y., Huh, J.-W., Jeong, K.-J., Har, D., Kwack, K.-S., Park, J.S., 2019. Rise of the Visible Monkey: Sectioned Images of Rhesus Monkey. Journal of Korean Medical Science 34. https://doi.org/10.3346/jkms.2019.34.e66

Goorley, T., James, M., Booth, T., Brown, F., Bull, J., Cox, L.J., Durkee, J., Elson, J., Fensin, M., Forster, R.A., Hendricks, J., Hughes, H.G., Johns, R., Kiedrowski, B., Martz, R., Mashnik, S., McKinney, G., Pelowitz, D., Prael, R., Sweezy, J., Waters, L., Wilcox, T., Zukaitis, T., 2016. Features of MCNP6. Annals of Nuclear Energy 87, 772–783. https://doi.org/10.1016/j.anucene.2015.02.020

ICRP, 2020. Paediatric Reference Computational Phantoms. ICRP Publication 143, Ann. ICRP.

ICRP, 2008. Nuclear Decay Data for Dosimetric Calculations. ICRP publication 107, Ann. ICRP 38.

Marti-Climent, J.M., Collantes, M., Jauregui-Osoro, M., Quincoces, G., Prieto, E., Bilbao, I., Ecay, M., Richter, J.A., Peñuelas, I., 2015. Radiation dosimetry and biodistribution in non-human primates of the sodium/iodide PET ligand [18F]-tetrafluoroborate. EJNMMI Res 5, 70. https://doi.org/10.1186/s13550-015-0148-5

Phillips, K.A., Bales, K.L., Capitanio, J.P., Conley, A., Czoty, P.W., 't Hart, B.A., Hopkins, W.D., Hu, S.-L., Miller, L.A., Nader, M.A., Nathanielsz, P.W., Rogers, J., Shively, C.A., Voytko, M.L., 2014. Why Primate Models Matter. Am J Primatol 76, 801–827. https://doi.org/10.1002/ajp.22281

Takamura, Y., Kajimoto, T., Tanaka, K., Yamamoto, T., Suzuki, M., Inaba, Y., Chida, K., Fukumoto, M., Rangacharyulu, C., Endo, S., 2023. Internal organ dose rate conversion coefficients of Japanese macaques to 134Cs,137Cs and 131I†. J Radiat Res 64, 804–810. https://doi.org/10.1093/jrr/rrad055

Villoing, D., Cuthbert, T.A., Kitahara, C.M., Lee, C., 2020. NCINM: organ dose calculator for patients undergoing nuclear medicine procedures. Biomed. Phys. Eng. Express 6, 055010. https://doi.org/10.1088/2057-1976/aba41e

Villoing, D., Kwon, T.-E., Pasqual, E., Kitahara, C.M., Lee, C., 2022. Organ dose calculator for diagnostic nuclear medicine patients based on the ICRP reference voxel phantoms and biokinetic models. Biomed Phys Eng Express 9. https://doi.org/10.1088/2057-1976/aca543

Weerts, E.M., Fantegrossi, W.E., Goodwin, A.K., 2007. The value of nonhuman primates in drug abuse research. Exp Clin Psychopharmacol 15, 309–327. https://doi.org/10.1037/1064-1297.15.4.309

Xie, T., Chen, X., Zaidi, H., 2020. Age-dependent dose calculations for common PET radionuclides and brain radiotracers in nonhuman primate computational models. Med Phys 47, 4465–4476. https://doi.org/10.1002/mp.14333

Table 1. List of source and target organs employed in the calculation of specific absorbed fractions for the monkey anatomical model

Serial Number	Organ name	Mass (g)	Serial Number	Organ name	Mass (g)
1	Skin	413.71	19	Urinary bladder	9.00
2	Fat	669.16	20	Urethra	0.12
3	Muscle	1784.41	21	Spleen	2.76
4	Skeleton	448.51	22	Lung	116.78
5	Tongue	9.13	23	Trachea	5.02
6	Stomach	482.72	24	Bronchus	3.51
7	Small intestine	360.14	25	Sclera	0.44
8	Liver	143.05	26	Vitreous humor	5.78
9	Large intestine	487.06	27	Lens cortex	0.08
10	Gall bladder	1.60	28	Lens nucleus	0.08
11	Esophagus	10.80	29	Cornea	0.02
12	Duodenum	13.82	30	Heart	48.53
13	Common bile duct	0.01	31	Brain	109.54
14	Adrenal gland	0.64	32	Breast	0.23
15	Thyroid gland	0.56	33	Kidneys	20.71
16	Ovary	0.40	34	Artery	7.41
17	Uterus	3.38	35	Vein	16.97
18	Vagina	3.02			

Table 2. S values (mGy/MBq-s) for Ga-68 calculated for ten major target and source organs of the monkey model

S values (mGy/MBq-s) for Ga-68	Source organs									
Target organs	Stomach	Small intestine	Liver	Large intestine	Esophagus	Urinary bladder	Lung	Heart	Kidney	Brain
Stomach	2.70E-04	1.03E-05	1.63E-05	2.41E-06	9.01E-06	3.87E-07	7.70E-06	7.46E-06	8.00E-06	7.76E-07
Small intestine	1.03E-05	3.56E-04	4.00E-06	1.07E-05	1.83E-06	1.10E-06	1.82E-06	1.67E-06	1.58E-05	4.21E-07
Liver	1.63E-05	3.99E-06	8.24E-04	1.97E-06	1.55E-05	3.00E-07	1.94E-05	1.63E-05	1.95E-05	1.07E-06
Large intestine	2.42E-06	1.07E-05	1.97E-06	2.58E-04	7.01E-07	1.61E-05	7.42E-07	6.31E-07	6.56E-06	2.01E-07
Esophagus	9.02E-06	1.81E-06	1.55E-05	6.93E-07	8.91E-03	1.42E-07	3.87E-05	2.95E-05	3.30E-06	4.11E-06
Urinary bladder	3.91E-07	1.11E-06	3.10E-07	1.60E-05	1.40E-07	1.09E-02	1.56E-07	1.50E-07	6.79E-07	4.39E-08
Lung	7.70E-06	1.82E-06	1.94E-05	7.42E-07	3.87E-05	1.60E-07	9.09E-04	5.30E-05	3.11E-06	2.13E-06
Heart	7.47E-06	1.67E-06	1.63E-05	6.33E-07	2.95E-05	1.44E-07	5.30E-05	2.41E-03	2.20E-06	1.81E-06
Kidney	7.98E-06	1.58E-05	1.95E-05	6.54E-06	3.29E-06	6.83E-07	3.12E-06	2.20E-06	5.23E-03	1.09E-06
Brain	7.56E-07	4.12E-07	1.05E-06	1.97E-07	4.09E-06	3.91E-08	2.12E-06	1.78E-06	1.08E-06	1.08E-03

Table 3. S values (mGy/MBq-s) for I-123 calculated for ten major target and source organs of the monkey model

S values (mGy/MBq-s) for I-123	Source organs									
Target organs	Stomach	Small intestine	Liver	Large intestine	Esophagus	Urinary bladder	Lung	Heart	Kidney	Brain
Stomach	1.82E-05	2.06E-06	3.08E-06	4.44E-07	1.68E-06	5.17E-08	1.56E-06	1.59E-06	1.70E-06	1.16E-07
Small intestine	2.07E-06	2.35E-05	7.72E-07	2.04E-06	3.23E-07	1.76E-07	3.14E-07	2.84E-07	3.31E-06	6.07E-08
Liver	3.15E-06	7.81E-07	4.96E-05	3.69E-07	3.47E-06	3.87E-08	3.52E-06	3.39E-06	3.19E-06	1.65E-07
Large intestine	4.44E-07	2.04E-06	3.64E-07	1.67E-05	1.08E-07	3.00E-06	1.13E-07	9.43E-08	1.17E-06	2.70E-08
Esophagus	1.66E-06	3.16E-07	3.34E-06	1.07E-07	4.78E-04	1.55E-08	7.30E-06	6.92E-06	6.06E-07	6.81E-07
Urinary bladder	5.22E-08	1.77E-07	3.77E-08	3.11E-06	1.62E-08	6.00E-04	1.84E-08	1.59E-08	9.85E-08	3.82E-09
Lung	1.59E-06	3.16E-07	3.53E-06	1.14E-07	7.62E-06	1.76E-08	5.14E-05	8.09E-06	5.73E-07	3.52E-07
Heart	1.61E-06	2.86E-07	3.37E-06	9.56E-08	7.14E-06	1.55E-08	8.01E-06	1.37E-04	3.86E-07	2.86E-07
Kidney	1.73E-06	3.38E-06	3.19E-06	1.19E-06	6.21E-07	9.75E-08	5.74E-07	3.85E-07	2.78E-04	1.83E-07
Brain	1.10E-07	5.78E-08	1.56E-07	2.56E-08	6.80E-07	3.48E-09	3.41E-07	2.73E-07	1.79E-07	6.38E-05

Table 4. S values (mGy/MBq-s) for I-123 calculated for ten major target and source organs of the monkey model

S values (mGy/MBq-s) for I-131	Source organs									
Target organs	Stomach	Small intestine	Liver	Large intestine	Esophagus	Urinary bladder	Lung	Heart	Kidney	Brain
Stomach	7.57E-05	3.80E-06	5.52E-06	9.62E-07	3.14E-06	1.49E-07	2.95E-06	3.06E-06	3.28E-06	3.06E-07
Small intestine	3.81E-06	9.99E-05	1.64E-06	3.72E-06	7.43E-07	4.43E-07	7.39E-07	6.78E-07	5.76E-06	1.64E-07
Liver	5.53E-06	1.64E-06	2.34E-04	8.00E-07	5.70E-06	1.15E-07	5.87E-06	5.76E-06	5.50E-06	4.25E-07
Large intestine	9.62E-07	3.72E-06	8.01E-07	7.28E-05	2.79E-07	4.99E-06	2.95E-07	2.49E-07	2.26E-06	7.69E-08
Esophagus	3.13E-06	7.35E-07	5.69E-06	2.74E-07	2.79E-03	5.31E-08	1.16E-05	1.13E-05	1.34E-06	1.66E-06
Urinary bladder	1.47E-07	4.44E-07	1.16E-07	4.99E-06	5.38E-08	3.37E-03	5.98E-08	5.47E-08	2.66E-07	1.42E-08
Lung	2.95E-06	7.39E-07	5.87E-06	2.93E-07	1.16E-05	5.85E-08	2.69E-04	1.29E-05	1.27E-06	8.56E-07
Heart	3.06E-06	6.78E-07	5.78E-06	2.50E-07	1.13E-05	5.29E-08	1.29E-05	6.75E-04	8.99E-07	7.27E-07
Kidney	3.28E-06	5.75E-06	5.51E-06	2.25E-06	1.34E-06	2.69E-07	1.27E-06	8.96E-07	1.51E-03	4.32E-07
Brain	2.97E-07	1.60E-07	4.15E-07	7.42E-08	1.64E-06	1.36E-08	8.47E-07	7.10E-07	4.27E-07	3.04E-04

Table 5. S values (mGy/MBq-s) for In-111 calculated for ten major target and source organs of the monkey model

S values (mGy/MBq-s) for In-111	Source organs									
Target organs	Stomach	Small intestine	Liver	Large intestine	Esophagus	Urinary bladder	Lung	Heart	Kidney	Brain
Stomach	2.83E-05	4.40E-06	6.43E-06	1.05E-06	3.60E-06	1.44E-07	3.39E-06	3.47E-06	3.73E-06	3.08E-07
Small intestine	4.40E-06	3.61E-05	1.81E-06	4.32E-06	8.02E-07	4.65E-07	7.93E-07	7.27E-07	6.86E-06	1.63E-07
Liver	6.49E-06	1.82E-06	7.12E-05	8.75E-07	7.01E-06	1.09E-07	7.14E-06	6.91E-06	6.53E-06	4.33E-07
Large intestine	1.05E-06	4.31E-06	8.71E-07	2.55E-05	2.86E-07	6.14E-06	3.01E-07	2.54E-07	2.58E-06	7.30E-08
Esophagus	3.57E-06	7.91E-07	6.88E-06	2.83E-07	5.96E-04	4.54E-08	1.47E-05	1.39E-05	1.45E-06	1.72E-06
Urinary bladder	1.44E-07	4.70E-07	1.08E-07	6.25E-06	4.68E-08	7.61E-04	5.21E-08	4.62E-08	2.70E-07	1.09E-08
Lung	3.42E-06	7.95E-07	7.14E-06	3.01E-07	1.50E-05	5.10E-08	6.90E-05	1.58E-05	1.38E-06	8.97E-07
Heart	3.49E-06	7.28E-07	6.91E-06	2.56E-07	1.41E-05	4.55E-08	1.58E-05	1.91E-04	9.72E-07	7.55E-07
Kidney	3.75E-06	6.90E-06	6.54E-06	2.60E-06	1.46E-06	2.68E-07	1.39E-06	9.68E-07	3.66E-04	4.48E-07
Brain	2.96E-07	1.56E-07	4.16E-07	6.96E-08	1.72E-06	1.06E-08	8.77E-07	7.27E-07	4.39E-07	9.17E-05

Table 6. S values (mGy/MBq-s) for Lu-177 calculated for ten major target and source organs of the monkey model

S values (mGy/MBq-s) for Lu-177	Source organs									
Target organs	Stomach	Small intestine	Liver	Large intestine	Esophagus	Urinary bladder	Lung	Heart	Kidney	Brain
Stomach	2.83E-05	4.40E-06	6.43E-06	1.05E-06	3.60E-06	1.44E-07	3.39E-06	3.47E-06	3.73E-06	3.08E-07
Small intestine	4.40E-06	3.61E-05	1.81E-06	4.32E-06	8.02E-07	4.65E-07	7.93E-07	7.27E-07	6.86E-06	1.63E-07
Liver	6.49E-06	1.82E-06	7.12E-05	8.75E-07	7.01E-06	1.09E-07	7.14E-06	6.91E-06	6.53E-06	4.33E-07
Large intestine	1.05E-06	4.31E-06	8.71E-07	2.55E-05	2.86E-07	6.14E-06	3.01E-07	2.54E-07	2.58E-06	7.30E-08
Esophagus	3.57E-06	7.91E-07	6.88E-06	2.83E-07	5.96E-04	4.54E-08	1.47E-05	1.39E-05	1.45E-06	1.72E-06
Urinary bladder	1.44E-07	4.70E-07	1.08E-07	6.25E-06	4.68E-08	7.61E-04	5.21E-08	4.62E-08	2.70E-07	1.09E-08
Lung	3.42E-06	7.95E-07	7.14E-06	3.01E-07	1.50E-05	5.10E-08	6.90E-05	1.58E-05	1.38E-06	8.97E-07
Heart	3.49E-06	7.28E-07	6.91E-06	2.56E-07	1.41E-05	4.55E-08	1.58E-05	1.91E-04	9.72E-07	7.55E-07
Kidney	3.75E-06	6.90E-06	6.54E-06	2.60E-06	1.46E-06	2.68E-07	1.39E-06	9.68E-07	3.66E-04	4.48E-07
Brain	2.96E-07	1.56E-07	4.16E-07	6.96E-08	1.72E-06	1.06E-08	8.77E-07	7.27E-07	4.39E-07	9.17E-05

Table 7. S values (mGy/MBq-s) for Tc-99m calculated for ten major target and source organs of the monkey model

S values (mGy/MBq-s) for Tc-99m	Source organs									
Target organs	Stomach	Small intestine	Liver	Large intestine	Esophagus	Urinary bladder	Lung	Heart	Kidney	Brain
Stomach	9.19E-06	1.34E-06	1.90E-06	3.45E-07	1.09E-06	4.57E-08	1.05E-06	1.09E-06	1.18E-06	9.85E-08
Small intestine	1.34E-06	1.18E-05	6.00E-07	1.30E-06	2.70E-07	1.56E-07	2.68E-07	2.47E-07	2.01E-06	5.16E-08
Liver	1.92E-06	6.05E-07	2.42E-05	2.88E-07	1.98E-06	3.39E-08	2.03E-06	2.00E-06	1.85E-06	1.40E-07
Large intestine	3.45E-07	1.29E-06	2.85E-07	8.42E-06	9.43E-08	1.71E-06	9.90E-08	8.36E-08	7.89E-07	2.27E-08
Esophagus	1.08E-06	2.64E-07	1.96E-06	9.24E-08	2.32E-04	1.32E-08	3.92E-06	3.82E-06	4.74E-07	5.44E-07
Urinary bladder	4.61E-08	1.57E-07	3.35E-08	1.73E-06	1.40E-08	2.88E-04	1.57E-08	1.37E-08	8.77E-08	3.21E-09
Lung	1.06E-06	2.69E-07	2.03E-06	9.93E-08	3.96E-06	1.50E-08	2.50E-05	4.24E-06	4.58E-07	2.85E-07
Heart	1.10E-06	2.49E-07	2.00E-06	8.46E-08	3.86E-06	1.31E-08	4.23E-06	6.58E-05	3.32E-07	2.47E-07
Kidney	1.19E-06	2.02E-06	1.85E-06	7.93E-07	4.82E-07	8.66E-08	4.58E-07	3.30E-07	1.34E-04	1.38E-07
Brain	9.28E-08	4.86E-08	1.31E-07	2.13E-08	5.40E-07	2.86E-09	2.75E-07	2.34E-07	1.33E-07	3.11E-05

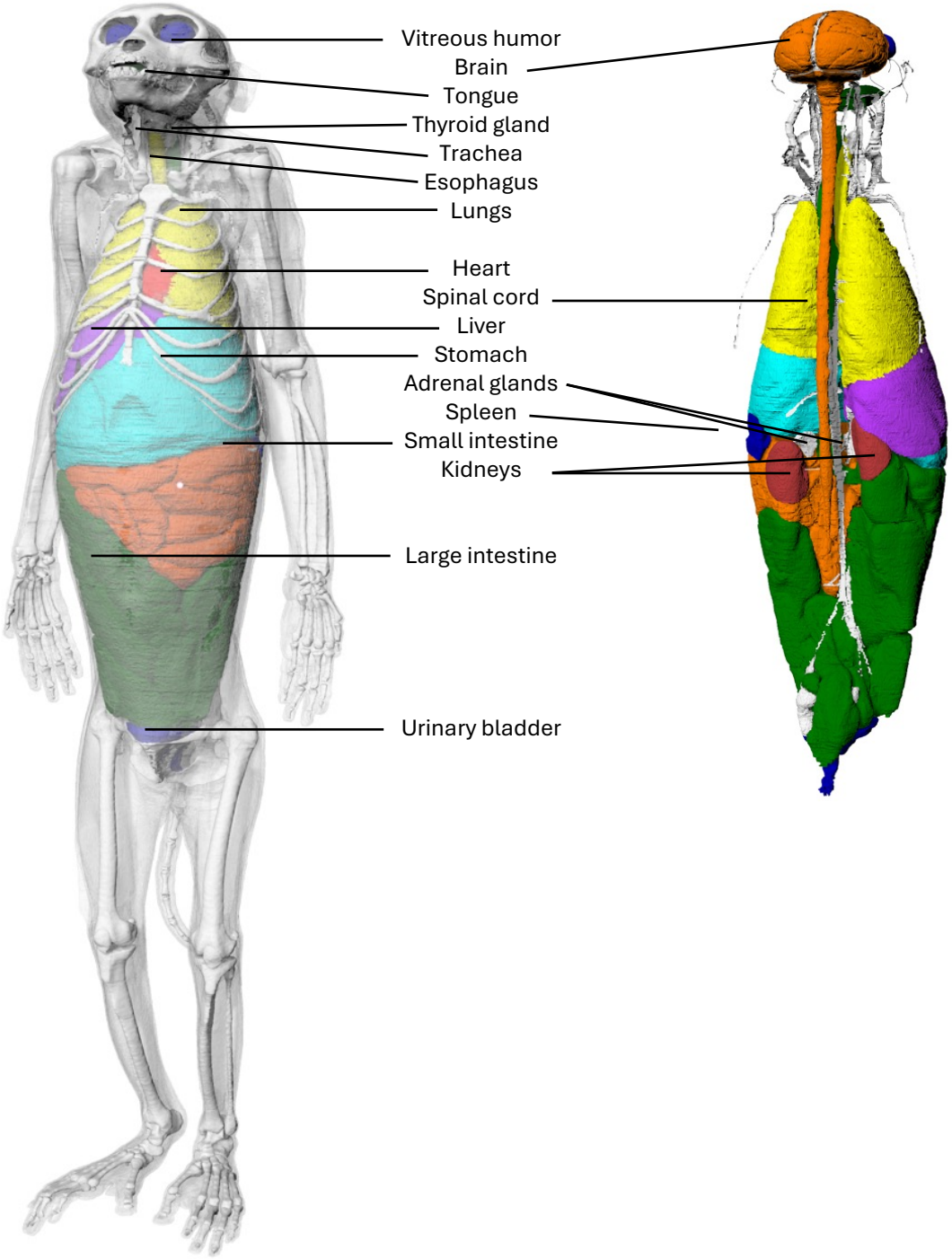

Figure 1. Frontal and rear views of the computational monkey model used for S value calculations

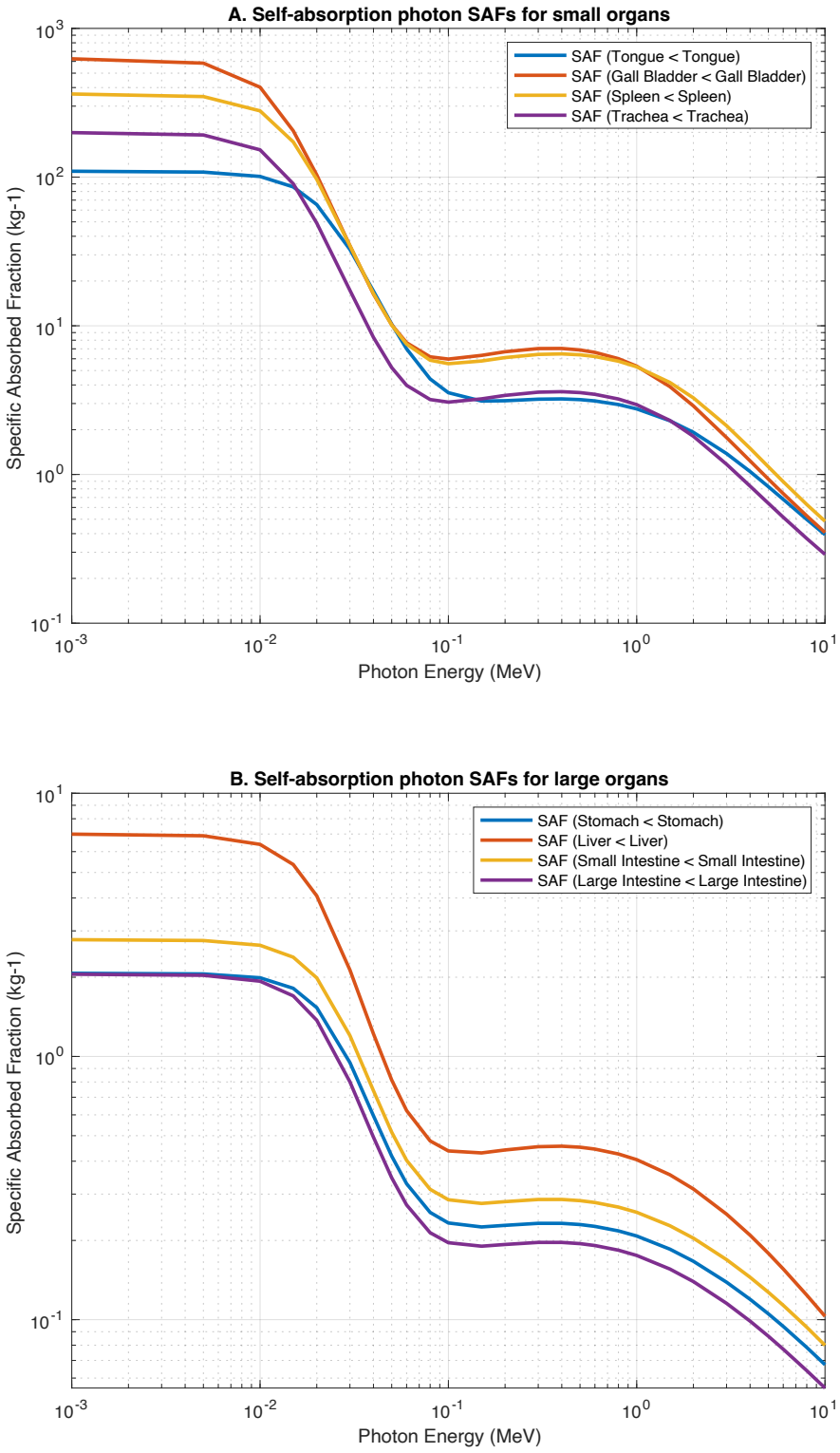

Figure 2. Self-absorption specific absorbed fractions (SAFs) for (a) small (<10 g) and (b) large organs (>100g).

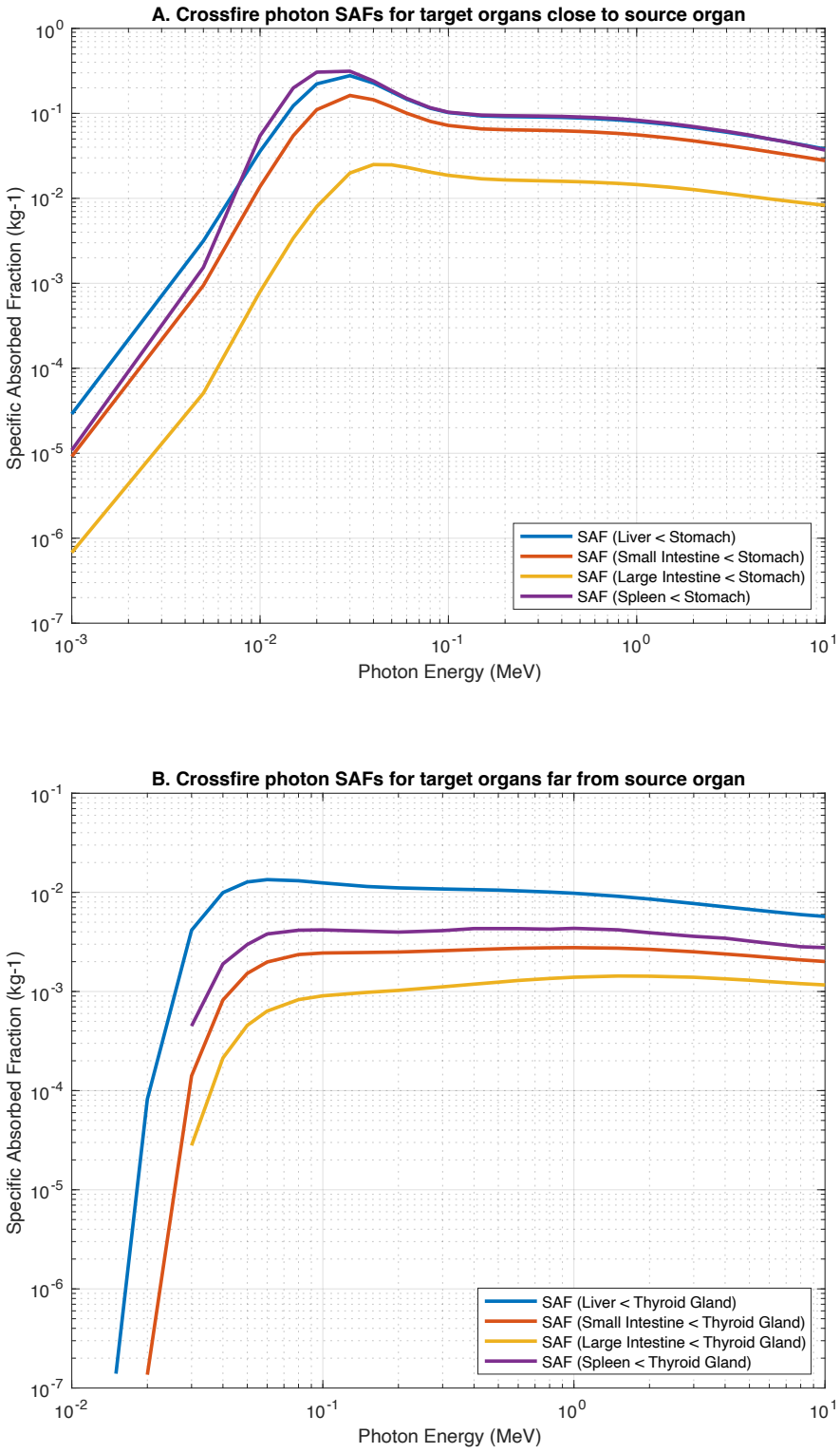

Figure 3. Crossfire specific absorbed fractions (SAFs) for target organs (a) close to and (b) far from source organs.

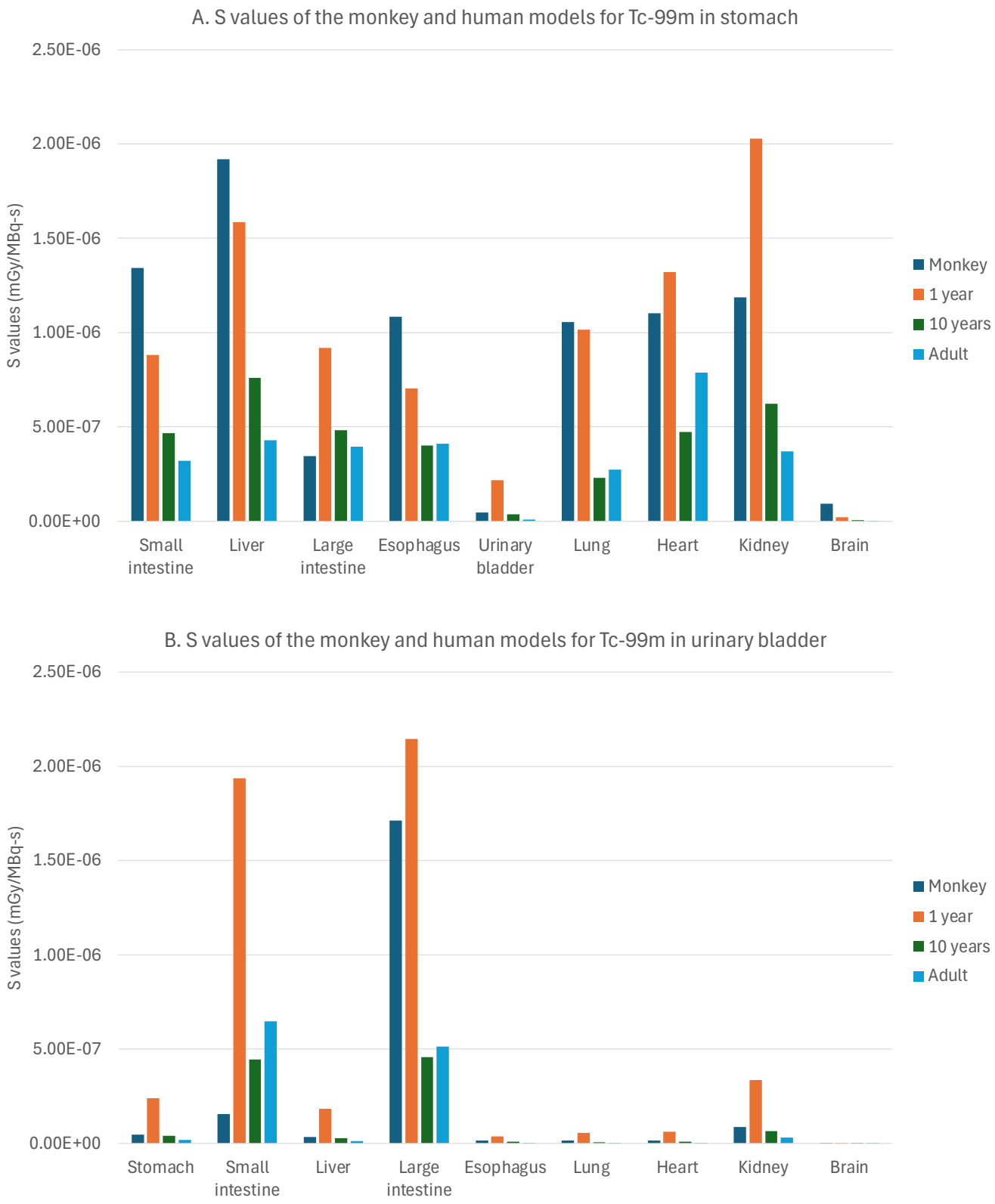

Figure 4. Comparison of S values when Tc-99m is distributed in (a) stomach and (b) urinary bladder between the monkey and human models (1 year, 10 years, and adult).